

# A novel computational approach to accelerate shading and blocking efficiency in solar tower power plants

**Linrui Guo**

College of Physics and Optoelectronic Engineering, Shenzhen 518060, China

LRGUO123@outlook.com

**Abstract.** This study presents a novel computational approach to enhance the efficiency of calculating shading and blocking in heliostat fields for solar tower power plants. Traditional methods for determining shading and blocking efficiency often involve substantial computational overhead due to the need to evaluate numerous heliostats within a field. To address this, our proposed method focuses on predicting potential heliostats that may cause shading or blocking, thereby significantly reducing the computation time and resource consumption. Through experimental validation, we demonstrate that our method maintains high computational accuracy and reliability while improving computational efficiency. This approach is critical for optimizing heliostat field layouts, ultimately leading to improved efficiency and reduced costs in solar tower power stations.

**Keywords:** Heliostat field, Solar tower power plants, Shading and blocking efficiency, Computational efficiency

## 1. Introduction

In response to the severe energy situation, the development and utilization of new energy sources have garnered global attention, holding significant importance for addressing energy depletion and increasingly severe environmental pollution issues. Solar energy, an inexhaustible renewable resource, plays a crucial role in this regard. Concentrating Solar Power (CSP), as a key technology in solar energy utilization [1-3], has promising prospects. It employs a concentrating system to collect solar energy and achieve high temperatures, which are used to heat the heat transfer medium. The heat accumulated in the heat transfer medium is then released in the power generation island to produce steam, driving a turbine, and consequently generating electricity.

Based on different concentrating methods, solar thermal power generation systems can be categorized into parabolic trough collectors, parabolic dish systems, solar towers, and linear Fresnel reflectors. Among these, the solar tower system has become a focal point of international attention due to its high concentration ratio, high power generation efficiency, advanced technology maturity, suitability for large-scale applications, and its capability to achieve continuous and stable power generation [4].

The tower solar thermal power generation system employs a vast array of heliostats that dynamically track the sun, focusing and reflecting sunlight onto a receiver atop the absorption tower, generating temperatures as high as 1000°C to heat the heat transfer medium within the receiver, thereby collecting solar thermal energy. The heliostat is a crucial component of the solar tower power station, representing

a significant proportion of the overall investment in the power plant. Studies suggest that the investment allocated to the heliostat field comprises between 40% to 50% of the total investment in the power plant [2, 5]. Furthermore, the design of the heliostat field directly affects the amount of energy received by the absorber, thus impacting the subsequent energy output [6]. Therefore, optimizing the layout of the heliostat field is of paramount importance for improving efficiency and reducing costs in solar tower power stations.

In the realm of optimizing heliostat field layouts, several studies have developed computational models such as DELSOL [7], Campo [8], MIRVAL [9], and HFLCAL [10], aimed at simulating the optical efficiency of heliostat fields. A typical heliostat field comprises thousands of heliostats, and traditional methods require extensive ray-tracing calculations. As a result, researchers have sought to develop methods that are both more precise and faster in calculating heliostat field efficiency. Cádiz et al. introduced an approach that optimizes the azimuthal distance between heliostats within a specific timeframe to precisely determine shading and blocking factors [11]. Besarati et al. proposed a technique for pinpointing heliostats with greatest likelihood of for shading and blocking, significantly reducing computation time [5]. Given the high computational costs and numerous variables in heliostat field optimization, computation time remains a primary limiting factor, with shading and blocking efficiency being major contributors to the computational load [12]. Consequently, this work proposes a method to predict potential heliostats that may cause shading and blocking of target heliostats, aiming to enhance computational efficiency. Specifically, this paper's principal contributions are outlined as follows:

1. We have identified the substantial computational burden involved in calculating shading and blocking efficiency, which limits the efficiency and scalability of current methods.
2. This study introduces a novel computational approach aimed at reducing the computational load associated with calculating shading and blocking efficiency. This method, based on the prediction of potential shading or blocking sources, significantly decreases computation time and resource consumption.
3. We have validated the proposed computational method and demonstrated its effectiveness in improving computational efficiency. Experimental results show that the new method not only significantly reduces the computational burden but also maintains high computational accuracy and reliability.

The rest of this paper is organized as follows: Section 2 describes the challenges in calculating shading and blocking efficiency; Section 3 introduces the method proposed in this work; Section 4 presents the experimental validation of the method's effectiveness; Section 5 summarizes the contributions of this paper.

## 2. Problem description

Various methods exist for calculating shading and blocking efficiency, such as MIEVAL [9], DELSOL [7], CAMPO [8], RCELL [13], SCT [14], and HFLD [15]. Computationally, these methods can be categorized into two types: planar projection [9, 13] and Monte Carlo ray tracing [16, 17]. Regardless of the method used, it is essential to first identify potential heliostats that may interfere with the selected heliostat (target heliostat) before calculating its shading and blocking efficiency. Without proper selection, the range of interfering heliostats would include all heliostats except the target one, an impractical approach due to the extensive traversal and judgment required, which are the main sources of computational overhead. This issue will be elaborated on later. Some scholars, after analyzing heliostat fields, have proposed methods to predict potential interfering heliostats that might affect the target heliostat. For example, the Besarati method sets a circular area with a certain radius centered on the target heliostat, considering heliostats within this area as potential interferers [5]. The Campo method identifies potential interfering heliostats based on layout characteristics [8]. While these methods are practical for predictions, they do not utilize the sun's position at a specific time, and their effectiveness and efficiency may vary with different application scenarios.

In the predictive method proposed in this work, we fully consider information such as the position of the sun and the dimensions of the heliostats to predict potential interfering heliostats. Since this predictive method better simulates the physical processes causing shading and blocking, it may exhibit better adaptability across different scenarios.

When sunlight is considered as parallel rays, the shadows and blocking effects caused by heliostats vary with the sun's position. With a fixed sun position, the projections of heliostats in planes of different spatial form polygons of various shapes. Calculating the exact projection of each heliostat in the field on the target heliostat to determine its shading and blocking efficiency would impose a significant computational burden. Therefore, it is crucial to first predict the potential interfering heliostats. This study employs a specific method to predict these potential interfering heliostats, which will be detailed in the method section.

### 3. Method

The power generation capability of a heliostat field is typically measured by its output thermal power. To simulate the power generation situation of a heliostat field, a mathematical model is now established to solve for its output thermal power.

#### 3.1. Models of heliostat field

The thermal power generated by heliostat field can be defined by:

$$E_{\text{field}} = \sum_i^N E_i = \text{DNI} \cdot \sum_i^N A_i \eta_{opt_i} \quad (1)$$

Where  $E_i$  is the thermal power output of the  $i^{\text{th}}$  heliostat,  $\text{DNI}$  is the direct normal irradiance;  $N$  is the total number of heliostats;  $A_i$  is the aperture area of the  $i^{\text{th}}$  heliostat;  $\eta_{opt_i}$  is the optical efficiency of the  $i^{\text{th}}$  heliostat.

One of the key parameters is the optical efficiency, which can be expressed by the following equation:

$$\eta_{opt} = \eta_{ref} \times \eta_{at} \times \eta_{cos} \times \eta_{int} \times \eta_{sb} \quad (2)$$

where  $\eta_{ref}$  is the specular reflectance,  $\eta_{at}$  is the atmospheric transmittance,  $\eta_{cos}$  is the cosine efficiency,  $\eta_{int}$  is the collector truncation efficiency and  $\eta_{sb}$  is the shadow shading efficiency.

##### 3.1.1. Heliostat reflectivity $\eta_{ref}$

Considering the reflectivity of the mirror material and the reduction in reflectivity due to diffuse reflection caused by dust deposition, among other factors [18], the effective reflectivity of the heliostat in this study is set as follows:

$$\eta_{ref} = 0.9082 \quad (3)$$

##### 3.1.2. Attenuation efficiency $\eta_{at}$

The intensity of the reflected light from the heliostat is attenuated by the scattering of atmospheric molecules, and the amount of attenuation is positively correlated with the distance of light transmission. This indicates that the attenuation efficiency decreases with increasing transmission distance, which can be accurately described by the following equation.

$$\begin{cases} \eta_{at} = 0.99321 - 0.0001176 \times d + 1.97 \times 10^{-8} \times d^2 (d \leq 1000\text{m}) \\ \eta_{at} = e^{-0.0001106 \times d} (d > 1000\text{m}) \end{cases} \quad (4)$$

where,  $d$  is the distance between the heliostat and the receiver.

##### 3.1.3. Cosine efficiency $\eta_{cos}$

The angle between the incident solar beam and the vector perpendicular to the heliostat surface determines the cosine efficiency. The cosine efficiency can be calculated by the dot product of two

vectors: the incident light vector  $\vec{l}$  from the sun to the center of the heliostat and the normal vector  $\vec{n}$  of the heliostat surface, according to the law of reflection:

$$-\vec{l} \cdot \vec{n} = |-\vec{l}| \cdot |\vec{n}| \cdot \cos \theta \quad (5)$$

It can be derived as:

$$\eta_{\cos} = \cos \theta = \frac{-\vec{l} \cdot \vec{n}}{|-\vec{l}| \cdot |\vec{n}|} = -\vec{l} \cdot \vec{n} \quad (6)$$

### 3.1.4. Interception efficiency $\eta_{int}$

Factors like surface roughness, tracking accuracy, and the sun's shape limit the amount of solar radiation that the receiver can capture from the heliostat's reflections. There are various methods to calculate the interception efficiency, including the HFLCAL model [10] and the UNIZAR model [19]. The HFLCAL model is significantly simpler and more precise compared to the UNIZAR model [20]. The HFLCAL model provides a method to calculate the interception efficiency of each heliostat, which can be evaluated using the formula below:

$$\eta_{int} = \frac{1}{2\pi\sigma_{tot}^2} \int_x \int_y \exp\left(-\frac{x^2 + y^2}{2\sigma_{tot}^2}\right) dydx \quad (7)$$

$\sigma_{tot}$  can be calculated as follows:

$$\sigma_{tot} = \sqrt{d^2(\sigma_{bq}^2 + \sigma_{track}^2 + \sigma_{sun}^2 + \sigma_{ast}^2)} \quad (8)$$

where,  $\sigma_{bq}$ ,  $\sigma_{track}$ ,  $\sigma_{sun}$ ,  $\sigma_{ast}$  represent the standard deviations attributed to the mirror slope error, the tracking error, the sun-shape error and the astigmatic effect, respectively.  $\sigma_{ast}$  can be calculated as follows:

$$\sigma_{ast} = \frac{\sqrt{0.5(H_t^2 + W_s^2)}}{4d} \quad (9)$$

$H_t$  and  $W_s$  can be computed as follows:

$$\begin{cases} H_t = \sqrt{LW \times LH} \left| \frac{d}{f} - \cos \theta \right| \\ W_s = \sqrt{LW \times LH} \left| \frac{d}{f} \cos \theta - 1 \right| \end{cases} \quad (10)$$

where  $LW$  and  $LH$  denote the width and length of a heliostat, respectively,  $\theta$  represents the incidence angle, and  $f$  equals  $d$ .

### 3.1.5. Shading and blocking efficiency $\eta_{sb}$

The shading and blocking efficiency consists of shading efficiency and blocking efficiency. When neighboring heliostats (referred to as question heliostats) block the incident light of the target heliostat, shadows are cast upon it, thereby reducing its effective reflective area and resulting in a decline in shading efficiency. When the reflected light of the target heliostat is blocked by question heliostats, the light cannot be effectively reflected to the receiver, resulting in a decrease in blocking efficiency.

### 3.2. Approach to identify potential question heliostats

The area and shape of the shadow indicate the heliostat's blocking effect on the light. The mutual shading relationship between heliostats can be determined based on the shadow's region. Therefore, potential question heliostats can be predicted by examining the shadow's extent. Since this involves predicting possible shading or blocking, it is unnecessary to derive the exact shadow extent. Instead, the maximum shadow extent can be used, which is much easier to compute and can be approximated as a rectangle.

(1) Calculate the maximum length ( $SL$ ) and width ( $SW$ ) of the heliostat's shadow based on the position of the sun.

$$\begin{cases} SL = \frac{HP + LH/2}{\tan \alpha} \\ SW = LW \end{cases} \quad (11)$$

where  $HP$  and  $\alpha$  are the height of heliostat pedestal and solar elevation angle, respectively.

(2) Adjust the maximum shadow range by appropriately enlarging it based on the dimensions of the heliostat.

$$\begin{cases} SL = LH + \frac{HP + LH/2}{\tan \alpha} \\ SW = 2LW \end{cases} \quad (12)$$

(3) Using the maximum shadow range to predict potential question heliostats causing shading.

To predict potential question heliostats causing shading, start from the center of the target heliostat, align with the midpoint of the width side of the rectangular shadow range, and extend the shadow range in the direction opposite to the incident light. Heliostats with centers falling within this range will be identified as potential question heliostats.

(4) Predicting potential question heliostats causing blocking.

To predict potential question heliostats causing blocking, start from the center of the target heliostat, align with the midpoint of the width side of the rectangular shadow range, and extend the shadow range in the direction of the target heliostat's reflected light. Heliostats with centers falling within this range will be identified as potential question heliostats.

#### 4. Experiment

To validate the effectiveness of the proposed method for predicting interfering heliostats in improving computational efficiency and reliability, we analyzed a heliostat field using both the algorithm presented in this work and a traditional search algorithm. This analysis included calculating each heliostat's atmospheric transmittance efficiency, annual average interception efficiency, cosine efficiency, shading and blocking efficiency, optical efficiency, and output power. The results obtained by the two methods, including their respective computation times and errors, were compared to demonstrate the model's reliability and computational efficiency.

##### 4.1. Parameter Settings

The basic parameters of a heliostat field are shown in Table 1 and layout of the heliostat field is depicted in figure 1.

To simplify calculations, all metrics denoted as "annual average" in this context are determined at local time points on the 21st of each month, specifically at 9:00, 10:30, 12:00, 13:30, and 15:00.

**Table 1.** Primary parameters of the heliostat utilized.

Parameter	Value	Unite
Latitude	39.4°N	-
Longitude	98.5°E	-
Tower optical height	80	m
Receiver height	8.0	m
Receiver radius	3.5	m
Heliostat total width	6.0	m
Heliostat total height	6.0	m
Heliostat pedestal height	4	m
Standard deviation of sun shape	2.51	mrاد
Standard deviation tracking error	0.63	mrاد
Standard deviation surface error	0.94	mrاد
Effective reflectivity	0.9082	-

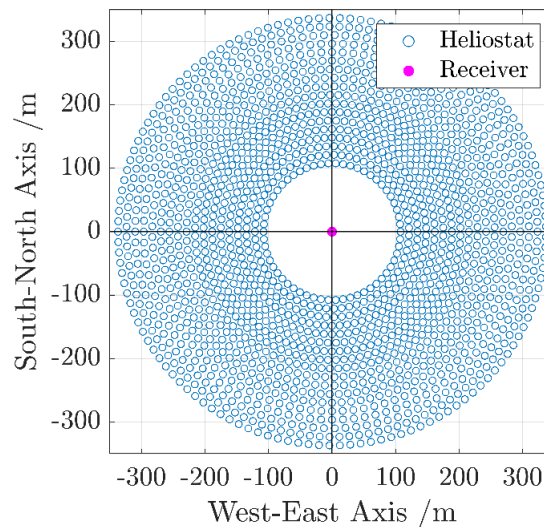


**Figure 1. Layout Diagram of the Heliostat Field.** A total of 1745 heliostats (blue circles) are arranged radially in a circular pattern, with the receiver (magenta dot) located at the center. The positive directions of the x-axis and y-axis represent the east and north directions, respectively.

#### 4.2. Results

Using the algorithm presented in this work, the above heliostat field was calculated, and the results were plotted as a heatmap of point clouds, as shown in figure 2. From figure 2(a), it can be observed that the atmospheric attenuation efficiency is determined by the distance between the heliostats and the receiver, with higher atmospheric transmittance efficiency for shorter distances. Since the heliostat field is located north of the Tropic of Cancer, sunlight always enters from its south throughout the year. Compared to heliostats in the south, heliostats in the north of the heliostat field receive sunlight directly for a longer duration throughout the year, resulting in higher annual average cosine efficiency. From figure 2(c), it can be seen that high values of annual average cosine efficiency are distributed in the northern part of the heliostat field, corresponding to the geographical location of the heliostat field. Moreover, they are symmetrically distributed in the east-west direction, as sunlight enters the heliostat field from both the west and east sides at equal durations during the day. Low values of shading and blocking efficiency are mainly distributed on heliostats located on the outer periphery of the northern part of the heliostat field. To redirect sunlight from the south to the receiver, these heliostats need to have larger tilt angles more often compared to other heliostats, increasing the likelihood of overlap in the projections within their planes with other heliostats, causing shadows or blockages. From figure 2(e-f), it can be observed that annual average optical efficiency and annual average output power are the combined results of atmospheric transmittance efficiency, interception efficiency, cosine efficiency, and shading and blocking efficiency.

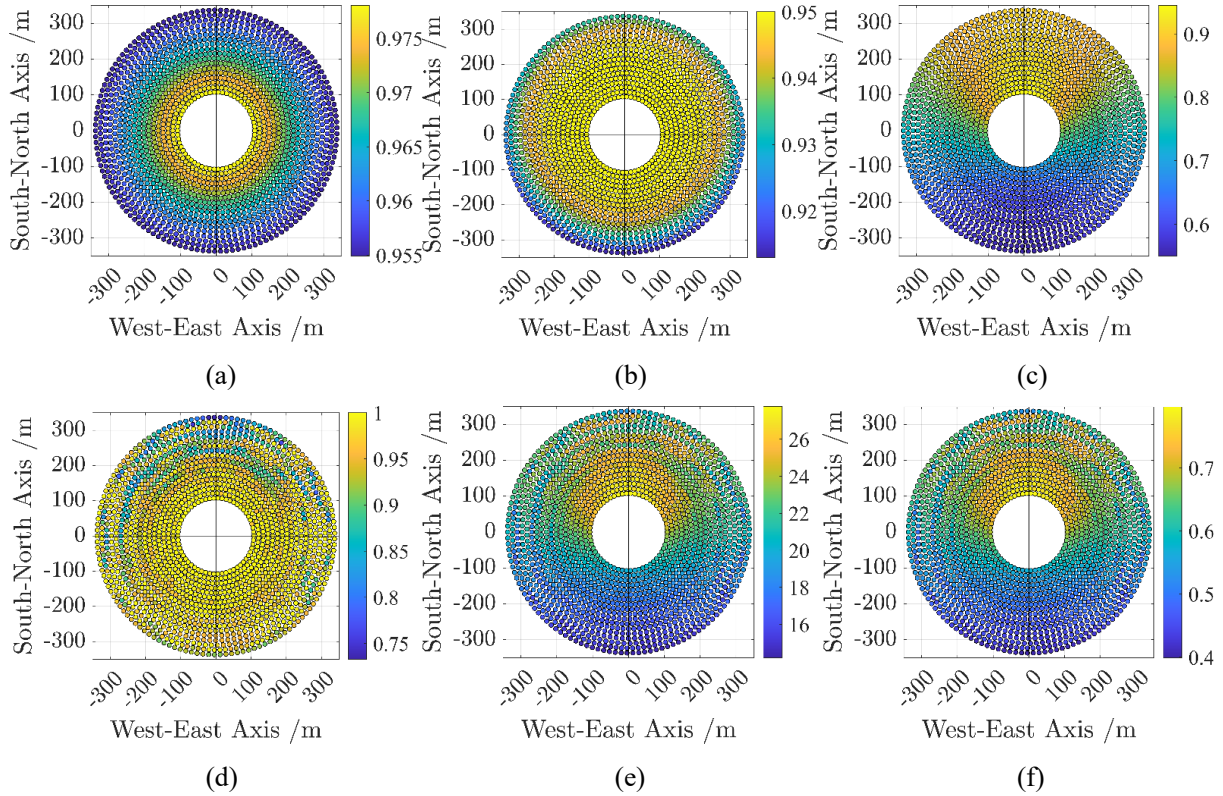


**Figure 2. Computation results point cloud heatmap.** This figure illustrates the outcomes of the calculations performed on the aforementioned heliostat field using the method proposed in this work. Colors represent the efficiency or power of the heliostats, with darker shades (deep blue) indicating lower values and lighter shades (bright yellow) indicating higher values. (a) Atmospheric transmittance efficiency of each heliostat (b) Annual average interception efficiency of each heliostat (c) Annual average cosine efficiency of each heliostat (d) Annual average shading and blocking efficiency of each heliostat (e) Annual average optical efficiency of each heliostat (f) Annual average output power of each heliostat (kW)

Using the search algorithm to solve the above heliostat field yielded a similar set of results. To compare the differences between the results obtained by the two methods, relative errors were used. The formula for calculating the relative error is as follows:

$$\delta = \frac{\Delta}{L} \cdot 100\% \quad (13)$$

where  $\Delta$  is the absolute error, equals to the value obtained by our method minus the value obtained by the search algorithm, and  $L$  is the value obtained by the search algorithm.

The relative errors for the values of each heliostat obtained by the two methods are shown in figure 3. From figure 3. (a-c), the relative errors for atmospheric transmittance efficiency, annual average interception efficiency, and annual average cosine efficiency of each heliostat are 0. This indicates that predicting potential interfering heliostats does not affect the calculation of these three parameters. The error distributions of annual average shading and blocking efficiency, optical efficiency, and output power for each heliostat are similar, with overall errors being small and randomly distributed. This suggests that the computational deviations for each heliostat do not show any obvious trends or patterns, reflecting the reliability of our algorithm.

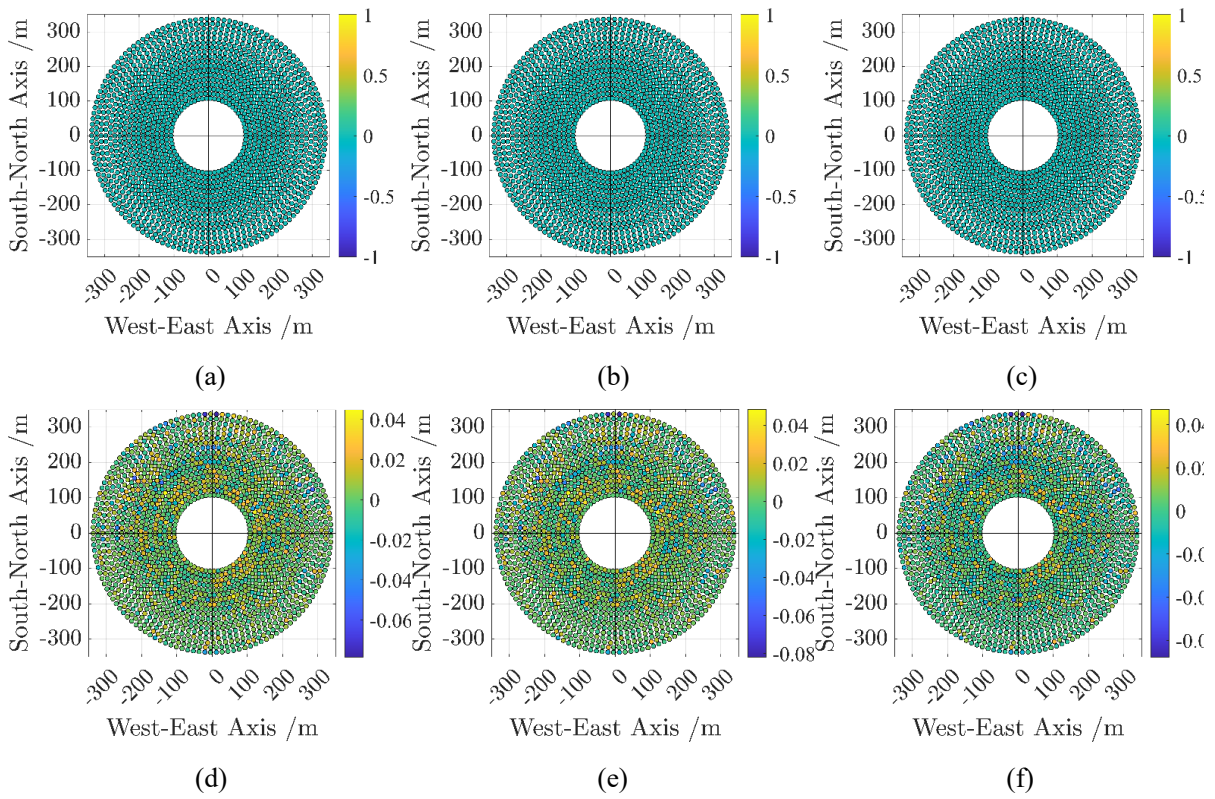


**Figure 3. The relative error point cloud heatmap.** The figure shows the relative errors between the results obtained using our method and the search algorithm. Colors represent the relative errors. (a) Relative error of atmospheric transmittance efficiency for each heliostat. (b) Relative error of annual average interception efficiency for each heliostat. (c) Relative error of annual average cosine efficiency for each heliostat. (d) Relative error of annual average shading and blocking efficiency for each heliostat. (e) Relative error of annual average optical efficiency for each heliostat. (f) Relative error of annual average output power for each heliostat.

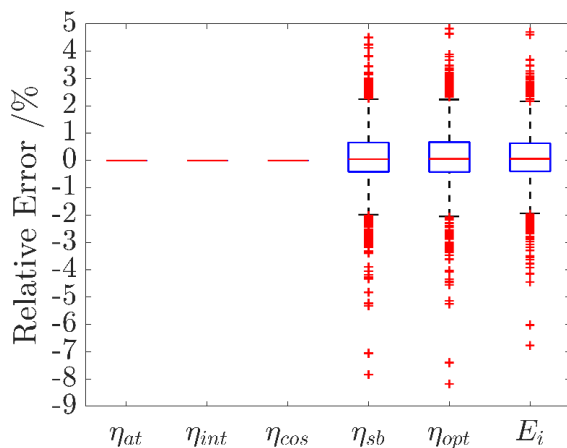


**Figure 4. The box plot of relative errors.** In a single box plot, from top to bottom, the lines represent the upper limit, upper quartile, median, and lower quartile, where the box formed by the upper and lower quartiles contains 50% of the data. The red plus signs indicate outliers in the data.

The results indicate that the proposed method demonstrates good computational accuracy and reliability. As shown in figure 4, the relative errors for atmospheric transmittance efficiency, annual average interception efficiency, and annual average cosine efficiency are zero. The box widths for the relative errors of annual average shading and blocking efficiency, optical efficiency, and output power

are similar. This similarity arises because the results of the shading and blocking efficiency calculations impact optical efficiency, which in turn affects output power. The number of outliers for these three parameters accounts for 5.9026%, 6.0745%, and 5.3868% of the total, respectively, with the maximum positive and negative relative errors not exceeding 5% and -9%. For annual average shading and blocking efficiency, 50% of the error data falls between 0.65139% and -0.41764%, with the maximum positive and negative relative errors being 4.5008% and -7.844%, respectively. These findings indicate that our method has good computational accuracy and reliability.

To compare the efficiency of the algorithms, both methods were used to solve the problem on the same computer, and the computation times for the complete solution processes were recorded.

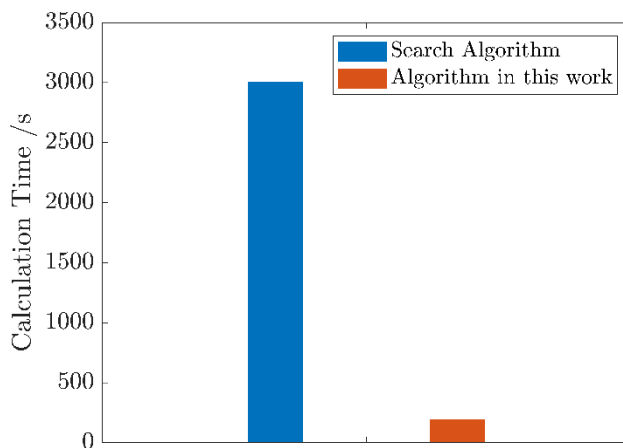


**Figure 5. Comparison between the computing time of the algorithm in this work and that of the search algorithm.** The computation times for our method and the search algorithm were 197.3703 seconds and 3008.3669 seconds, respectively.

From figure 5, it can be seen that our method reduces the computation time by 93.4393%, significantly reducing the calculation time.

## 5. Conclusions

In this study, we propose a new computational method for calculating the shading and blocking efficiency of heliostat fields in solar thermal power generation systems. We have identified that traditional methods face significant computational burdens when calculating shading and blocking efficiency. The method proposed in this study effectively reduces computation time and resource consumption. Experimental results show that the new method not only has significant advantages in improving computational efficiency but also maintains high computational accuracy and reliability.

## References

- [1] LIU Q, BAI Z, SUN J, *et al.* Thermodynamics investigation of a solar power system integrated oil and molten salt as heat transfer fluids [J]. *Applied Thermal Engineering*, 2016, 93: 967-77.
- [2] PIROOZMAND P, BOROUSHAKI M. A computational method for optimal design of the multi-tower heliostat field considering heliostats interactions [J]. *Energy*, 2016, 106: 240-52.
- [3] XU C, WANG Z, LI X, *et al.* Energy and exergy analysis of solar power tower plants [J]. *Applied Thermal Engineering*, 2011, 31(17): 3904-13.
- [4] BEHAR O, KHELLAF A, MOHAMMEDI K. A review of studies on central receiver solar thermal power plants [J]. *Renewable and Sustainable Energy Reviews*, 2013, 23: 12-39.
- [5] BESARATI S M, YOGI GOSWAMI D. A computationally efficient method for the design of the heliostat field for solar power tower plant [J]. *Renewable Energy*, 2014, 69: 226-32.
- [6] WEI X, LU Z, YU W, *et al.* A new code for the design and analysis of the heliostat field layout for power tower system [J]. *Solar Energy*, 2010, 84(4): 685-90.
- [7] KISTLER B L. A user's manual for DELSOL3: a computer code for calculating the optical performance and optimal system design for solar thermal central receiver plants [R]: Sandia National Lab.(SNL-CA), Livermore, CA (United States), 1986.

- [8] COLLADO F J, GUALLAR J. Campo: Generation of regular heliostat fields [J]. *Renewable Energy*, 2012, 46: 49-59.
- [9] LEARY P L H, J. D. User's guide for MIRVAL: a computer code for comparing designs of heliostat-receiver optics for central receiver solar power plants [J]. *Central Receivers*, 1979.
- [10] SCHWARZBÖZL P, PITZ-PAAL R, SCHMITZ M. Visual HFLCAL - A Software Tool for Layout and Optimisation of Heliostat Fields [M]. 2009.
- [11] CÁDIZ P, FRASQUET M, SILVA M, *et al.* Shadowing and blocking effect optimization for a variable geometry heliostat field [J]. *Energy procedia*, 2015, 69: 60-9.
- [12] WANG J, DUAN L, YANG Y. An improvement crossover operation method in genetic algorithm and spatial optimization of heliostat field [J]. *Energy*, 2018, 155: 15-28.
- [13] LIPPS F. Shading and blocking geometry for a solar tower concentrator with rectangular mirrors; proceedings of the American society of mechanical engineers, winter annual meeting, F, 1974 [C].
- [14] SÁNCHEZ M, ROMERO M. Methodology for generation of heliostat field layout in central receiver systems based on yearly normalized energy surfaces [J]. *Solar Energy*, 2006, 80(7): 861-74.
- [15] WEI X, LU Z, LIN Z, *et al.* Optimization procedure for design of heliostat field layout of a 1MWe solar tower [J]. *Solid State Lightning and Solar Energy Technologies, Photonics Asia*, 2007.
- [16] WENDELIN T. SolTRACE: a new optical modeling tool for concentrating solar optics; proceedings of the International solar energy conference, F, 2003 [C].
- [17] NOONE C J, TORRILHON M, MITSOS A. Heliostat field optimization: A new computationally efficient model and biomimetic layout [J]. *Solar Energy*, 2012, 86(2): 792-803.
- [18] COLLADO F J, GUALLAR J. A review of optimized design layouts for solar power tower plants with campo code [J]. *Renewable and Sustainable Energy Reviews*, 2013, 20: 142-54.
- [19] COLLADO F J, GÓMEZ A, TURÉGANO J A. An analytic function for the flux density due to sunlight reflected from a heliostat [J]. *Solar Energy*, 1986, 37(3): 215-34.
- [20] COLLADO F J. One-point fitting of the flux density produced by a heliostat [J]. *Solar Energy*, 2010, 84(4): 673-84.